Journal of Nonlinear Modeling and Analysis
Volume 8, Number 1, February 2026, 72–93
https://global-sci.com/jnma
DOI:10.12150/jnma.2026.72

MEK Inhibition May Prevent the Recruitment of NK Cells in the Tumor Microenvironment: A Mathematical Model of Glioma Treatment

Amine Alabkari[1,†], Ahmed Kourrad[1] and Khalid Adnaoui[1]

Received 17 December 2024; Accepted 12 August 2025

Abstract In this paper, we analyze the dynamics of oncolytic virotherapy combined with MEK inhibitors for the treatment of glioma. Although the therapeutic effect of oncolytic viruses (OV) depends on the recruitment of NK cells, these viruses are frequently subject to NK cell clearance, which may reduce the efficacy of oncolytic virotherapy. Furthermore, it is more challenging for OV to enter glioma cells because these cells lack Coxsackievirus and Adenovirus Receptors (CAR). MEK inhibitors, however, are able to compensate for this deficiency in CAR molecules. Herein, we propose and analyze a mathematical model of the dynamics of cancer cells, oncolytic viruses, activated NK cells, and CAR molecules while combining oncolytic virotherapy with MEK inhibition. Our goal is to identify the circumstances in which the treatment may be effective. In this research, we investigated the existence of equilibrium points. The two endemic equilibriums and the virus infection-free equilibrium stability conditions are given. The findings demonstrate that, in a dynamical system, NK cell activation can either establish or destroy equilibrium points and that substantial recruitment of activated NK cells might have detrimental effects on oncolytic virotherapy. However, MEK inhibitors boost OV effectiveness and may prevent NK cell recruitment.

Keywords Glioma, cancer, oncolytic virotherapy, MEK inhibitors, mathematical model

MSC(2010) 92C50, 34D20, 92C37, 37N25.

1. Introduction

In a number of preclinical and clinical tumor models, oncolytic virotherapy has demonstrated promising antitumoral effects [1–4]. An oncolytic virus (OV) that selectively replicates to kill cancer cells while preserving healthy normal cells is used in this therapy strategy. Additionally, oncolytic virotherapy promotes a strong immune response to both infected and uninfected tumors [2, 5, 6]. However, oncolytic viruses are frequently susceptible to immune cell clearance when supplied through a

[†]the corresponding author.
Email address: aminealabkari@gmail.com (A. Alabkari), ahmedkourrad@gmail.com (A. Kourrad), khalid.adnaoui@gmail.com (K. Adnaoui)
[1]Laboratory of Analysis Modeling and Simulation, Faculty of Sciences Ben M'Sik, Hassan II University, BP 7955, Sidi Othman, Casablanca, Morocco.

vein to immunocompetent hosts. This lowers the chances of virotherapeutic success [7, 8].

Natural killer (NK) cells and T lymphocytes are well-known to have a significant role in oncolytic virotherapy. Wodarz et al. [9] demonstrated that for OV to have a therapeutic impact, NK cells and T cells are necessary. Senekal et al. [10] investigated how oncolytic virotherapy was affected by the recruitment of NK cells. Their findings demonstrate the critical functions that OV infection plays in reducing tumor growth and activating a potent NK cell response to achieve tumor remission. However, other studies [11–13] showed that the impact of virotherapy on the eradication of tumor cell populations may be diminished. Virus-induced immune responses may also destroy virus-infected tumor cells prematurely, before viruses have a chance to produce new progeny.

In our research, we are interested in the dynamics of OV therapy for glioma and how it interacts with NK cell recruitment. We only take into account the newly emerging function of NK cells in oncolytic virotherapy due to the need for a more thorough investigation of their dual and counter-intuitive contributions [8].

Gliomas are a type of brain cancer that arise from cells that help support the brain's neurons [14]. Major research on the use of several oncolytic viruses in the treatment of gliomas has been done [15, 16]. Adenoviral vectors have an edge over other viral vectors because they are comparatively non-toxic and do not integrate into the genome [17]. However, the lack of Coxsackievirus and Adenovirus Receptors (CAR) on the surface of gliomas makes it difficult for wild-type adenoviral vectors to effectively transduce in these tumors [18]. Studies from clinical trials have demonstrated that the absence or diminished expression of CAR in tumor cells, particularly in glioma cells, complicates the entry of an adenovirus into these cells [18]. Targeting the adenovirus to gliomas remains difficult because the CAR levels in gliomas are low [16].

Mitogen-activated protein kinase kinase (MEK) inhibitors have been shown to increase CAR expression [19]. However, MEK inhibitors may limit the replication of the virus. This requires finding an optimal balance between the positive effect of MEK inhibitors and their negative effect. This makes the dynamics of the group consisting of tumor cells, viruses, and MEK inhibitors more complicated. Zurakowski and Wodarz [19] proposed an ODE model to describe the effects of MEK inhibitors and viruses on tumor cells. They used it to investigate whether the combined therapy may reduce the size of the tumor. More recently, Camara et al. [20] analytically demonstrated the conditions that lead to optimal therapy in minimizing glioma cells proliferation using a spatiotemporal mathematical model that describes the interaction between tumor cells and oncolytic viruses. They stated that when the amount of MEK inhibitors is high, virotherapy always fails. However, the dynamics of CAR expression on the cells' surface were not included in their model. Recently, Nono et al. [21] proposed a nonlinear mathematical model of brain tumor control through regulating the growth of cancer cells by employing conditionally replicative adenoviruses (CRAds) and MEK inhibitors in combination therapy. But they didn't take into account the recruitment of NK cells into the tumor microenvironment.

In this paper, we propose a mathematical model of the dynamical interactions among cancer cells, oncolytic viruses, virus-induced NK cells, and CAR molecules. Particularly, our study aims to analyze how the combination of MEK inhibitors and activated NK cells affects oncolytic virotherapy.

2. Mathematical model

We present the mathematical model describing the dynamics of glioma treatment with oncolytic adenoviruses over time. The model that we use in our work is an extension of those presented in [13] and with the following modifications: (1) Infection needs interaction of free virus with a CAR receptor on a susceptible cancer cell which requires adding a new variable C that represents the average number of CAR molecules on the surface of the cells. (2) Glioma is treated using oncolytic virotherapy combined with MEK inhibition. The model includes five variables: activated NK cells (N), uninfected cancer cells (U), infected cancer cells (I), free virus particles (V) and the average number of CAR molecules on the surface of the cells (C). It is given by the following set of differential equations which describes the development of these sub-populations over time:

$$\begin{cases} \frac{dN}{dt} = \alpha NI - d_1 N, & (2.1.a) \\ \frac{dU}{dt} = r(1-\xi)U\left(1 - \frac{U+I}{K}\right) - \beta CUV - \lambda_1 NU, & (2.1.b) \\ \frac{dI}{dt} = \beta CUV - d_2(1-\xi)I - \lambda_2 NI, & (2.1.c) \\ \frac{dV}{dt} = bd_2(1-\xi)I - \beta CUV - d_3 V, & (2.1.d) \\ \frac{dC}{dt} = \eta\xi(m-C) - d_4 C. & (2.1.e) \end{cases} \tag{2.1}$$

In Eq. (2.1.a), α is the activation rate of the NK cells by infected cancer cells and d_1 is the clearance rate of NK cells.

In Eq. (2.1.b), the term $r(1-\xi)U\left(1 - \frac{U+I}{K}\right)$ represents the logistic tumor growth where r is the intrinsic growth rate of the tumor, K is the carrying capacity tumor size, and ξ represents the efficiency of MEK inhibitors in reducing tumor growth. The factor $(1-\xi)$ directly reduces the intrinsic growth rate r, with higher values of ξ indicating greater therapeutic efficacy and resulting in a more pronounced reduction in tumor proliferation due to the inhibitory action of the treatment. The expression $U+I$ denotes the total tumor cell population, under the assumption that both uninfected (U) and infected (I) cells contribute to tumor growth. The term βCUV describes the rate of infected cells through interaction of free virus with a CAR receptor on a susceptible cancer cell. The decay rate of uninfected cancer cells due to activated NK cells is expressed by $-\lambda_1 NU$.

In Eq. (2.1.c), the term $-d_2 I$ is the natural death rate of infected tumor cells and $-\lambda_2 NI$ is the decay rate of infected tumor cells due to activated NK cells.

In Eq. (2.1.d), the term $bd_2 I$ represents the virus proliferation rate where the virus burst size is b, whereas d_3 is the clearance rate of the virus.

In Eq. (2.1.e), we assume that CAR is produced by cells with a rate η, and production is related to inhibitor activity ξ [21]. That is, the stronger the inhibitor activity, the higher the production rate of CAR. The term $m - C$ represents the saturation of CAR expression. That is, the cell cannot bear an infinite number of receptors, but production declines and stops as their number on the cell surface increases. CAR is lost from the cell surface with a rate d_4.

Symbol	Description	Value	Range	Reference
r	Tumor cell growth rate	0.5 day^{-1}	0.12 - 1.2	[22]
K	Tumor cell carrying capacity	2×10^9 cells	10^9 - 2×10^9	[23]
β	Viral infection rate	1.2×10^{-10} $pfu^{-1}.day^{-1}$	4×10^{-12} - 1.26×10^{-10}	[24]
α	Activation rate of the NK cells	1.3×10^{-7} $cell^{-1}.day^{-1}$	-	[15]
ξ	Efficiency of MEK inhibitors	0.6	0 - 1	[19, 20]
λ_1	Killing rate of cancer cells by NK cells	6.9×10^{-6} NK $cell^{-1}.day^{-1}$	-	[25]
λ_2	Killing rate of infected cancer cells by NK cells	6.9×10^{-5} NK $cell^{-1}.day^{-1}$	-	[25]
d_1	Clearance rate of NK cells	9.8×10^{-2} day^{-1}	-	[25]
d_2	Death rate of infected cells	10 day^{-1}	0.0034 - 11	[26]
b	Burst size of infected cells	1000 $pfu.cell^{-1}$	0 - 1000	[22, 24]
d_3	Viral clearance rate	24 day^{-1}	0.24 - 24	[22, 24]
η	Production rate of CAR	0.17 day^{-1}	-	[21]
m	Maximum number of CAR on cell surface	2	1 - 10	[21]
d_4	Loss rate of CAR from the cell surface	0.07 day^{-1}	-	[21]

Table 1. Parameters and constants

3. Positivity and boundedness

- **Positivity**

  Let us show that if the initial conditions of system (2.1) are non-negative, then the solution remains non-negative for all time. Assume the initial conditions

satisfy $N(0), U(0), I(0), V(0), C(0) \geq 0$. Then evaluating each equation at the zero boundary gives:

$$\begin{aligned}
\left.\frac{dN}{dt}\right|_{N=0} &= 0, \\
\left.\frac{dU}{dt}\right|_{U=0} &= 0, \\
\left.\frac{dI}{dt}\right|_{I=0} &= \beta\, C\, U\, V \geq 0, \\
\left.\frac{dV}{dt}\right|_{V=0} &= b\, d_2(1-\xi)\, I \geq 0, \\
\left.\frac{dC}{dt}\right|_{C=0} &= \eta\, \xi\, m \geq 0.
\end{aligned}$$

Since each derivative is non-negative on the corresponding boundary plane of the non-negative orthant, the vector field points either inward or tangentially along the boundary [27]. Consequently, by standard results in dynamical systems (e.g., the inward-pointing vector field criterion for positively invariant sets), the non-negative region is positively invariant.

- **Boundedness**

1) From (2.1.b) + (2.1.c), we can see that:

$$\begin{aligned}
\frac{d}{dt}(U+I) &= r(1-\xi)U\left(1-\frac{U+I}{K}\right) - d_2(1-\xi)I - \lambda_2 N I - \lambda_1 N U \\
&\leq r(1-\xi)U\left(1-\frac{U+I}{K}\right) \\
&\leq r(1-\xi)(U+I)\left(1-\frac{U+I}{K}\right).
\end{aligned}$$

Let $W = U + I$. We derive:

$$\frac{d}{dt}W \leq r(1-\xi)\, W\left(1-\frac{W}{K}\right).$$

Consider the logistic equation

$$\frac{d}{dt}w = r(1-\xi)\, w(1-w/K),$$

with initial condition $w(0) = W(0)$. The following properties hold [28]:

- If $0 \leq w(0) \leq K$, then $w(t)$ stays in $[0, K]$ for all t.
- Moreover, $w(t)$ converges to K as $t \to \infty$.

By classical comparison theory for ODEs [29], we have:

$$W(t) \leq w(t) \quad \text{for all } t \geq 0.$$

Since $w(t) \to K$ as $t \to \infty$, it follows that:

$$\limsup_{t\to\infty} W(t) \leq \limsup_{t\to\infty} w(t) = K.$$

2) From (2.1.d), we have:

$$\begin{aligned}\frac{dV}{dt} &= b(1-\xi)d_2 I - \beta CUV - d_3 V \\ &\leq b(1-\xi)d_2 I - d_3 V \\ &\leq b(1-\xi)d_2(U+I) - d_3 V \\ &\leq b(1-\xi)d_2 K - d_3 V.\end{aligned}$$

This yields the linear differential inequality:

$$\frac{dV}{dt} + d_3 V \leq b(1-\xi)d_2 K.$$

To solve this, we multiply both sides by the integrating factor $e^{d_3 t}$:

$$e^{d_3 t}\frac{dV}{dt} + d_3 e^{d_3 t} V \leq b(1-\xi)d_2 K e^{d_3 t}.$$

The left-hand side is the derivative of $V(t)e^{d_3 t}$:

$$\frac{d}{dt}\left(V(t)e^{d_3 t}\right) \leq b(1-\xi)d_2 K e^{d_3 t}.$$

Integrate both sides from 0 to t:

$$V(t)e^{d_3 t} - V(0) \leq \frac{b(1-\xi)d_2 K}{d_3}\left(e^{d_3 t} - 1\right).$$

Multiply through by $e^{-d_3 t}$ and rearrange:

$$V(t) \leq V(0)e^{-d_3 t} + \frac{b(1-\xi)d_2 K}{d_3}\left(1 - e^{-d_3 t}\right).$$

Taking the limit superior as $t \to \infty$ (and noting that $e^{-d_3 t} \to 0$):

$$\limsup_{t\to\infty} V(t) \leq \frac{b(1-\xi)d_2 K}{d_3}.$$

3) Similarly, from (2.1.e), we have:

$$\begin{aligned}\frac{dC}{dt} &= \eta\xi(m - C) - d_4 C \\ &= \eta\xi m - \eta\xi C - d_4 C \\ &= \eta\xi m - (\eta\xi + d_4)C.\end{aligned}$$

This gives the linear differential equation:

$$\frac{dC}{dt} + (\eta\xi + d_4)C = \eta\xi m.$$

To solve that, we multiply by $e^{(\eta\xi + d_4)t}$:

$$e^{(\eta\xi+d_4)t}\frac{dC}{dt} + (\eta\xi + d_4)e^{(\eta\xi+d_4)t}C = \eta\xi m e^{(\eta\xi+d_4)t}.$$

The left-hand side is the derivative of $C(t)e^{(\eta\xi+d_4)t}$:

$$\frac{d}{dt}\left(C(t)e^{(\eta\xi+d_4)t}\right) = \eta\xi m e^{(\eta\xi+d_4)t}.$$

Integrating both sides from 0 to t:

$$C(t)e^{(\eta\xi+d_4)t} - C(0) = \frac{\eta\xi m}{\eta\xi+d_4}\left(e^{(\eta\xi+d_4)t}-1\right).$$

Multiplying through by $e^{-(\eta\xi+d_4)t}$ yields:

$$C(t) = C(0)e^{-(\eta\xi+d_4)t} + \frac{\eta\xi m}{\eta\xi+d_4}\left(1-e^{-(\eta\xi+d_4)t}\right).$$

Taking the limit as $t\to\infty$ (since $e^{-(\eta\xi+d_4)t}\to 0$):

$$\lim_{t\to\infty} C(t) = \frac{\eta\xi m}{\eta\xi+d_4}.$$

We conclude that the set

$$\left\{(N,U,I,V,C)\in\mathbb{R}^5_+ \mid U+I\le K,\ V\le\frac{b(1-\xi)d_2K}{d_3},\ C\le\frac{\eta\xi m}{\eta\xi+d_4}\right\}$$

is a positively invariant set and an attracting region for the model system (2.1).

4. Virus infection-free equilibrium

Let $\widetilde{x}(\widetilde{N},\widetilde{U},\widetilde{I},\widetilde{V},\widetilde{C})$ be an arbitrary equilibrium point. The corresponding Jacobian matrix is given by :

$$\mathcal{J}_{\widetilde{x}} = \begin{pmatrix} \alpha\widetilde{I}-d_1 & 0 & \alpha\widetilde{N} & 0 & 0 \\ -\lambda_1\widetilde{U} & \widetilde{\Gamma} & \frac{-r(1-\xi)}{K}\widetilde{U} & -\beta\widetilde{C}\widetilde{U} & -\beta\widetilde{U}\widetilde{V} \\ -\lambda_2\widetilde{I} & \beta\widetilde{C}\widetilde{V} & -(1-\xi)d_2-\lambda_2\widetilde{N} & \beta\widetilde{C}\widetilde{U} & \beta\widetilde{U}\widetilde{V} \\ 0 & -\beta\widetilde{C}\widetilde{V} & b(1-\xi)d_2 & -\beta\widetilde{C}\widetilde{U}-d_3 & -\beta\widetilde{U}\widetilde{V} \\ 0 & 0 & 0 & 0 & -\eta\xi-d_4 \end{pmatrix}$$

with $\widetilde{\Gamma} = r(1-\xi)\left(1-\frac{\widetilde{U}+\widetilde{I}}{K}\right) - \frac{r(1-\xi)}{K}\widetilde{U} - \beta\widetilde{C}\widetilde{V} - \lambda_1\widetilde{N}$.

We make the right side of the system (2.1) equal to 0. There are two feasible infection-free equilibrium $E_0 = (0,0,0,0,C_0)$ and $E_1 = (0,K,0,0,C_0)$ where $C_0 = \frac{\eta\xi m}{\eta\xi+d_4}$.

The corresponding Jacobian matrix at E_0 is given by

$$\mathcal{J}_{E_0} = \begin{pmatrix} -d_1 & 0 & 0 & 0 & 0 \\ 0 & r(1-\xi) & 0 & 0 & 0 \\ 0 & 0 & -(1-\xi)d_2 & 0 & 0 \\ 0 & 0 & b(1-\xi)d_2 & -d_3 & 0 \\ 0 & 0 & 0 & 0 & -\eta\xi-d_4 \end{pmatrix}.$$

It is obvious that, E_0 is unstable due to the positive eigenvalue r. On the other hand, the corresponding Jacobian matrix at E_1 is given by

$$\mathcal{J}_{E_1} = \begin{pmatrix} -d_1 & 0 & 0 & 0 & 0 \\ -\lambda_1 K & -r(1-\xi) & -r(1-\xi) & -\beta K C_0 & 0 \\ 0 & 0 & -(1-\xi)d_2 & \beta K C_0 & 0 \\ 0 & 0 & b(1-\xi)d_2 & -\beta K C_0 - d_3 & 0 \\ 0 & 0 & 0 & 0 & -\eta\xi - d_4 \end{pmatrix}$$

and, since the eigenvalues $\rho_1 = -d_1$, $\rho_2 = -r(1-\xi)$ and $\rho_3 = -\eta\xi - d_4$ are negative, then the stability of E_1 depends on the stability of the sub-matrix:

$$\mathcal{J}'_{E_1} = \begin{pmatrix} -(1-\xi)d_2 & \beta K C_0 \\ b(1-\xi)d_2 & -\beta K C_0 - d_3 \end{pmatrix}. \tag{4.1}$$

The matrix $\mathcal{J}'_{E_1}$ is stable if its determinant is non-negative since its trace is clearly negative. This condition is equivalent to $\mathcal{R}_0 < 1$ where $\mathcal{R}_0 = \sqrt{\frac{b\beta K C_0}{\beta K C_0 + d_3}}$ is the basic reproduction number of the system (2.1). To compute the basic reproduction number $\mathcal{R}_0$ using the Next Generation Matrix method, we can follow these steps:

- **Step 1** (Identify Infected Compartments):

  The compartments involved in new infections and infectious progression are:

  I : infected cancer cells;
  V: free virus particles.

- **Step 2** (Define $\mathcal{F}$ and $\mathcal{V}$):

  Let $\mathbf{x} = (I, V)^T$ be the vector of infected states.
  We write the system as:

  $$\frac{d\mathbf{x}}{dt} = \mathcal{F}(\mathbf{x}) - \mathcal{V}(\mathbf{x}),$$

  where:
  $\mathcal{F}$: new infections;
  $\mathcal{V}$: transfer between compartments.

- **Step 3** (Extract $\mathcal{F}$ and $\mathcal{V}$):

  From system (2.1):

  $$\mathcal{F} = \begin{pmatrix} \beta C U V \\ b d_2 (1-\xi) I \end{pmatrix},$$

  $$\mathcal{V} = \begin{pmatrix} d_2(1-\xi)I + \lambda_2 N I \\ \beta C U V + d_3 V \end{pmatrix}.$$

- **Step 4** (Compute F and V Jacobians of $\mathcal{F}$ and $\mathcal{V}$ respectively at the infection-free equilibrium E_1):

We compute the Jacobians:

$$F = D\mathcal{F}|_{E_1} = \begin{pmatrix} 0 & \beta C_0 K \\ bd_2(1-\xi) & 0 \end{pmatrix},$$
$$V = D\mathcal{V}|_{E_1} = \begin{pmatrix} d_2(1-\xi) & 0 \\ 0 & \beta C_0 K + d_3 \end{pmatrix}.$$

- **Step 5** (Compute FV^{-1}):

$$FV^{-1} = \begin{pmatrix} 0 & \beta C_0 K \\ bd_2(1-\xi) & 0 \end{pmatrix} \cdot \begin{pmatrix} \frac{1}{d_2(1-\xi)} & 0 \\ 0 & \frac{1}{\beta C_0 K + d_3} \end{pmatrix}$$
$$= \begin{pmatrix} 0 & \frac{\beta C_0 K}{\beta C_0 K + d_3} \\ b & 0 \end{pmatrix}.$$

- **Step 6** ($\mathcal{R}_0$ is equal to the spectral radius (largest eigenvalue)):

$$\mathcal{R}_0 = \rho(FV^{-1}) = \sqrt{\frac{b\beta K C_0}{\beta K C_0 + d_3}}.$$

Theorem 4.1. *The virus infection-free equilibrium E_1 is locally asymptotically stable if $\mathcal{R}_0 < 1$, and it is unstable if $\mathcal{R}_0 > 1$.*

5. Endemic equilibrium

Let us determine in which conditions the system (2.1) admits an endemic equilibrium (N^*,U^*, I^*,V^*,C^*) where $I^* > 0$ and $V^* > 0$. We make the right side of the system (2.1) equal to 0 which is rearranged to obtain the following:

- If $N^* = N_1 = 0$, the resulting expressions from equations (1.b), (1.c), and (1.d) are given by:

$$\begin{aligned} &\text{(i)} \quad r(1-\xi)U^*\left(1 - \frac{U^* + I^*}{K}\right) = \beta C^* U^* V^*, \\ &\text{(ii)} \quad \beta^* U^* V^* = d_2(1-\xi)I^*, \\ &\text{(iii)} \quad bd_2(1-\xi)I^* = \beta C^* U^* V^* + d_3 V^*, \\ &\text{(iv)} \quad C^* = C_0. \end{aligned}$$

From equations (ii) and (iii), we obtain:

$$bd_2(1-\xi)I^* = d_2(1-\xi)I^* + d_3 V^*.$$

Solving for V^*, we find :

$$V^* = V_1 = \frac{(b-1)(1-\xi)d_2}{d_3} I^*.$$

Substituting this expression for V^* into equation (ii) and simplifying yields:

$$U^* = U_1 = \frac{d_3}{\beta C_0(b-1)}.$$

Finally, by substituting U^*, V^*, and C^* in (i), we obtain:

$$I^* = I_1 = \frac{K - \frac{d_3}{\beta C_0(b-1)}}{\frac{\beta K C_0(b-1)d_2}{r d_3} + 1}.$$

Hence, the endemic equilibrium $E_2(N_1, U_1, I_1, V_1, C_0)$ exists if $K - \frac{d_3}{\beta C_0(b-1)} > 0$ which is equivalent to $\mathcal{R}_0 > 1$.

- If $N^* = N_2 \neq 0$, then $I^* = I_2 = a_1$, $N^* = N_2 = a_2 - a_3 V_2$, $U^* = U_2 = K(a_4 + a_5 V_2) - a_1$ and $C^* = C_0$ where $a_1 = \frac{d_1}{\alpha}$, $a_2 = \frac{(b-1)(1-\xi)d_2}{\lambda_2}$, $a_3 = \frac{\alpha d_3}{\lambda_2 d_1}$, $a_4 = 1 - \frac{\lambda_1(b-1)d_2}{r\lambda_2}$ and $a_5 = \frac{\alpha\lambda_1 d_3 - \beta C_0 \lambda_2 d_1}{r(1-\xi)\lambda_2 d_1}$. By substituting in (2.1.c) and putting the right side equal to 0, we obtain:

$$V^* = V_2 = \frac{-\beta C_0 a_4 - a_1 a_3 \lambda_2 + \sqrt{(\beta C_0 a_4 + a_1 a_2 \lambda_2)^2 + 4\beta C_0(a_1 d_2 + a_1 a_2 \lambda_2)a_5}}{2\beta C_0 a_5}.$$

Theorem 5.1. *The NK cell-free equilibrium $E_2(N_1, U_1, I_1, V_1, C_0)$ is an asymptotically stable endemic equilibrium if $\mathcal{R}_0 > 1$.*

Proof. Since the Jacobian matrix $\mathcal{J}_{E_2}$ evaluated at $\mathcal{R}_0 = 1$ and $b = b^* = \frac{\beta K C_0 + d_3}{\beta K C_0}$ has a simple zero eigenvalue while all the other eigenvalues are negative, the system undergoes a non-hyperbolic bifurcation. In such cases, linearization is insufficient to determine the local dynamics, and the application of center manifold theory [30] becomes necessary to reduce the system to a lower-dimensional system that captures the behavior near the bifurcation point. To determine the direction and stability of the bifurcation, we compute two key coefficients:

- π_1 associated with the nonlinear curvature of the reduced system [30], and
- π_2 which measures the sensitivity to changes in the bifurcation parameter b.

Let F denote the vector field defined by the right side of system (2.1), and define the state variables as $N = x_1$, $U = x_2$, $I = x_3$, $V = x_4$ and $C = x_5$. The coefficients π_1 and π_2 are computed from the second-order partial derivatives of F, evaluated at the bifurcation point. The left eigenvector $[v_1, v_2, v_3, v_4, v_5]$ and the right eigenvector $[w_1, w_2, w_3, w_4, w_5]^T$ of $\mathcal{J}_{E_2}$ corresponding to the zero eigenvalue, are given by:

$$v_1 = 0,\ v_2 = 0,\ v_3 = b^*,\ v_4 = 1,\ v_5 = 0,$$

$$w_1 = 0,\ w_2 = -\frac{1}{(1-\xi)d_2} - \frac{1}{r(1-\xi)},\ w_3 = \frac{1}{(1-\xi)d_2},\ w_4 = \frac{1}{\beta K C_0} \text{ and } w_5 = 0.$$

The right eigenvector spans the center manifold, representing the direction along which perturbations evolve near the bifurcation. The left eigenvector serves to project the nonlinear dynamics onto this manifold, enabling us to quantify how system nonlinearities influence stability.

Then, the coefficients π_1 and π_2 are computed as:

$$\pi_1 = \sum_{k,i,j=1}^{5} v_k w_i w_j \left(\frac{\partial^2 F_k}{\partial x_i \partial x_j}\right)_{(E_2,b^*)},$$
$$\pi_2 = \sum_{k,i=1}^{5} v_k w_i \left(\frac{\partial^2 F_k}{\partial x_i \partial b}\right)_{(E_2,b^*)}.$$

Only v_3 and v_4 are nonzero, so the two expressions simplify to:

$$\begin{aligned}
\pi_1 &= b^* \sum_{i,j=1}^{5} w_i w_j \left(\frac{\partial^2 F_3}{\partial x_i \partial x_j}\right)_{(E_2,b^*)} + \sum_{i,j=1}^{5} w_i w_j \left(\frac{\partial^2 F_4}{\partial x_i \partial x_j}\right)_{(E_2,b^*)} \\
&= b^* \sum_{i,j=2}^{4} w_i w_j \left(\frac{\partial^2 F_3}{\partial x_i \partial x_j}\right)_{(E_2,b^*)} + \sum_{i,j=2}^{4} w_i w_j \left(\frac{\partial^2 F_4}{\partial x_i \partial x_j}\right)_{(E_2,b^*)} \\
&= 2b^* \beta C_0 w_2 w_4 - 2\beta C_0 w_2 w_4 \\
&= 2(b^* - 1)\beta C_0 w_2 w_4 \\
&= -\frac{2(b^* - 1)(r + d_2)}{rKd_2} < 0, \\
\pi_2 &= b^* \sum_{i=1}^{5} w_i \left(\frac{\partial^2 F_3}{\partial x_i \partial b}\right)_{(E_2,b^*)} + \sum_{i=1}^{5} w_i \left(\frac{\partial^2 F_4}{\partial x_i \partial b}\right)_{(E_2,b^*)} \\
&= w_3 \left(\frac{\partial^2 F_4}{\partial x_3 \partial b}\right)_{(E_2,b^*)} \\
&= (1 - \xi) d_2 w_3 \\
&= 1 > 0.
\end{aligned}$$

Since $\pi_1 < 0$ and $\pi_2 > 0$, from Theorem 4.1 in [31], the endemic equilibrium E_2 is locally asymptotically stable if $\mathcal{R}_0 > 1$. □

Theorem 5.2. *The presence of NK cells equilibrium $E_3(N_2, U_2, I_2, V_2, C_0)$ is asymptotically stable if $A_0 > 0$, $A_1 > 0$, $A_2 > 0$, $A_3 > 0$, $A_4 > 0$, $A_3A_4 > A_2$ and $A_2(A_3A_4 - A_2) > A_4(A_1A_4 - A_0)$.*

Proof. The corresponding Jacobian matrix at E_3 is given by

$$\mathcal{J}_{E_3} = \begin{pmatrix}
0 & 0 & \alpha N_2 & 0 & 0 \\
-\lambda_1 U_2 & \Gamma & \frac{-r(1-\xi)}{K} U_2 & -\beta C_0 U_2 & -\beta U_2 V_2 \\
-\lambda_2 I_2 & \beta C_0 V_2 & -(1-\xi)d_2 - \lambda_2 N_2 & \beta C_0 U_2 & \beta U_2 V_2 \\
0 & -\beta C_0 V_2 & b(1-\xi)d_2 & -\beta C_0 U_2 - d_3 & -\beta U_2 V_2 \\
0 & 0 & 0 & 0 & -\eta\xi - d_4
\end{pmatrix}$$

with $\Gamma = r(1-\xi)\left(1 - \frac{U_2+I_2}{K}\right) - \frac{r(1-\xi)}{K} U_2 - \beta C_0 V_2 - \lambda_1 N_2$. The characteristic equation, which determines the eigenvalues of the Jacobian matrix, is:

$$\rho^5 + A_4\rho^4 + A_3\rho^3 + A_2\rho^2 + A_1\rho + A_0 = 0,$$

where

$$
\begin{aligned}
A_4 &= -r(1-\xi)\left(1-\tfrac{U_2+I_2}{K}\right)+\tfrac{r(1-\xi)}{K}U_2+\beta C_0\left(U_2+V_2\right)+\left(\lambda_2+\lambda_1\right)N_2+\eta\xi+d_2+d_3+d_4,\\
A_3 &= -b(1-\xi)d_2\beta C_0U_2+\left(d_2+\lambda_2N_2\right)\left(\beta C_0U_2+d_3\right)-\Big[r(1-\xi)\left(1-\tfrac{U_2+I_2}{K}\right)-\tfrac{r(1-\xi)}{K}U_2\\
&\quad -\beta C_0V_2-\lambda_1N_2-\eta\xi-d_4\Big]+\left((1-\xi)d_2+\lambda_2N_2+\beta C_0U_2+d_3\right)-\beta C_0V_2\left(\tfrac{r(1-\xi)}{K}U_2-\beta C_0U_2\right)\\
&\quad +\alpha\lambda_2I_2N_2,\\
A_2 &= -\Gamma\left[\left((1-\xi)d_2+\lambda_2N_2\right)\left(\beta C_0U_2+d_3\right)-b(1-\xi)d_2\beta C_0U_2\right]\\
&\quad -\left(\eta\xi+d_4\right)\left[\Gamma\left((1-\xi)d_2+\lambda_2N_2+\beta C_0U_2+d_3\right)\right.\\
&\quad \left.-\left((1-\xi)d_2+\lambda_2N_2\right)\left(\beta C_0U_2+d_3\right)+b(1-\xi)d_2\beta C_0U_2\right]+\alpha N_2\lambda_2I_2\left(\eta+d_4\right)\\
&\quad -\beta C_0V_2\Big[\left(\eta+d_4\right)\left(\tfrac{r(1-\xi)}{K}U_2-\beta C_0U_2\right)+\tfrac{r(1-\xi)}{K}U_2d_3+\beta C_0U_2\left((b-1)(1-\xi)d_2-\lambda_2N_2\right)\Big]\\
&\quad -\alpha N_2\Big[\lambda_1U_2\beta C_0V_2-\lambda_2I_2\left(\tfrac{r(1-\xi)}{K}U_2+\beta C_0V_2+\lambda_1N_2+\beta C_0U_2+d_3\right)\Big],\\
A_1 &= -\left(\eta\xi+d_4\right)\left[\Gamma\left(\left(\left(1-\xi\right)d_2+\lambda_2N_2\right)\left(\beta C_0U_2+d_3\right)-b(1-\xi)d_2\beta C_0U_2\right)\right.\\
&\quad \left.+\tfrac{r(1-\xi)}{K}U_2d_3+\beta C_0U_2\left((b-1)(1-\xi)d_2-\lambda_2N_2\right)\right]\\
&\quad -\alpha N_2\Big[\left(\lambda_1U_2\beta C_0V_2\right)\left(2\beta C_0U_2+d_3\right)-\lambda_2I_2\left(\left(\tfrac{r(1-\xi)}{K}U_2+\beta C_0V_2+\lambda_1N_2\right)\left(\beta C_0U_2+d_3\right)-\beta^2C_0^2U_2V_2\right)\Big]\\
&\quad +\alpha N_2\left(\eta\xi+d_4\right)\left(-\lambda_1U_2\beta C_0V_2+\lambda_2I_2\left(\tfrac{r(1-\xi)}{K}U_2+\beta C_0V_2+\lambda_1N_2+\beta C_0U_2+d_3\right)\right),\\
A_0 &= \alpha N_2\left(\eta\xi+d_4\right)\left[-\lambda_1U_2\beta C_0V_2\left(2\beta C_0U_2+d_3\right)\right.\\
&\quad \left.+\lambda_2I_2\left(\left(\tfrac{r(1-\xi)}{K}U_2+\beta C_0V_2+\lambda_1N_2\right)\left(\beta C_0U_2+d_3\right)-\beta^2C_0^2U_2V_2\right)\right].
\end{aligned}
$$

By the Routh-Hurwitz criterion, $E_3(N_2,U_2,I_2,V_2,C_0)$ is asymptotically stable if $A_0>0$, $A_1>0$, $A_2>0$, $A_3>0$, $A_4>0$, $A_3A_4>A_2$ and $A_2\left(A_3A_4-A_2\right)>A_4\left(A_1A_4-A_0\right)$. □

6. Sensitivity analysis of the basic reproduction number

Here, we evaluate how the model's parameters affect the reproduction number $\mathcal{R}_0$. We carry it out by calculating the $\mathcal{R}_0$ elasticity indices (see Table 2) with respect to the parameter values listed in Table 1. According to the method suggested in [32], the expression of $\mathcal{R}_0$ elasticity index with respect to a parameter p, where p is any of the parameters listed in Table 1, is provided by

$$
S_{\mathcal{R}_0}^{p}=\left(\frac{\partial\mathcal{R}_0}{\partial p}\right)\left(\frac{p}{\mathcal{R}_0}\right).
$$

Parameter p	Derivative $\frac{\partial \mathcal{R}_0}{\partial p}$	Elasticity index $S^p_{\mathcal{R}_0}$
b	$\frac{\beta K C_0}{2\mathcal{R}_0(\beta K C_0+d_3)}$	5×10^{-1}
K	$\frac{b d_3 \beta C_0}{2\mathcal{R}_0(\beta K C_0+d_3)^2}$	4.94×10^{-1}
β	$\frac{b d_3 K C_0}{2\mathcal{R}_0(\beta K C_0+d_3)^2}$	4.94×10^{-1}
d_3	$\frac{-b\beta K C_0}{2\mathcal{R}_0(\beta K C_0+d_3)^2}$	-4.94×10^{-1}
d_4	$\frac{-b\beta K\eta\xi m d_3}{2\mathcal{R}_0(\beta K\eta\xi m+d_3(\eta\xi+d_4))^2}$	-2.01×10^{-1}
η	$\frac{b\beta K\xi m d_3 d_4}{2\mathcal{R}_0(\eta\xi+d_4)^2(\beta K C_0+d_3)^2}$	2.01×10^{-1}
m	$\frac{b\beta K\eta d_3}{2\mathcal{R}_0(\eta\xi+d_4)(\beta K C_0+d_3)^2}$	8.24×10^{-1}
ξ	$\frac{b\beta K\eta m d_3 d_4}{2\mathcal{R}_0(\eta\xi+d_4)^2(\beta K C_0+d_3)^2}$	2.01×10^{-1}

Table 2. Elasticity indexes of the basic reproduction number $\mathcal{R}_0$

These indices can pinpoint crucial parameters for cancer control since they quantify the ratio of relative changes on $\mathcal{R}_0$ in response to corresponding changes in the parameters. The elasticity indices of $\mathcal{R}_0$ to the model's parameters are shown in Table 2. We find that the reproduction number is the most sensitive to maximum number of CAR on cell surface (m), with an elasticity index of 0.82. This means that increasing CAR expression significantly enhances immune detection and viral infection efficiency. A 1% increase in m results in a 0.82% increase in $\mathcal{R}_0$, suggesting that therapeutic strategies (like for example increasing the effectiveness of MEK inhibitors) that boost CAR density on cell surfaces could substantially impact disease dynamics. The burst size (b), with an elasticity of 0.5, also plays a key role. This reflects the number of new viruses produced per lysed infected cell. A larger burst size allows the virus to spread more efficiently within the tumor, potentially accelerating immune-mediated clearance. This indicates the importance of optimizing oncolytic viruses for maximal replication and release. Next, parameters such as the tumor carrying capacity (K), the viral infection rate (β), and the viral clearance rate (d_3) all exhibit high elasticity values (± 0.49). This suggests a delicate balance: increasing β or K favors viral spread and higher $\mathcal{R}_0$, potentially enhancing tumor clearance. Conversely, higher d_3 (faster virus removal) suppresses $\mathcal{R}_0$, possibly hindering therapy success. Moderate elasticity values are observed for the efficiency of MEK inhibitors (ξ), the production rate of CARs on the cell surface (η), and the loss rate of CARs (d_4), each with an elasticity index around ± 0.2. These findings suggest that:

- Increasing the MEK inhibitor efficiency (ξ) moderately boosts $\mathcal{R}_0$, implying that more effective MEK inhibition could enhance viral replication or immune activation by making tumor cells more susceptible to infection or recognition.
- Enhancing the production rate of CARs (η) increases $\mathcal{R}_0$, indicating that therapies aimed at upregulating CAR expression could improve immune engagement and treatment efficacy.
- Reducing the loss rate of CARs from the cell surface (d_4) also supports higher $\mathcal{R}_0$, underscoring the importance of CAR stability and retention on tumor cells for sustaining immune targeting and viral entry.

Although their individual elasticities are lower than those of m, b, or β, these parameters still exert biologically meaningful control. Therefore, therapeutic strategies that combine CAR enhancement, MEK inhibition, and viral optimization could synergistically elevate $\mathcal{R}_0$ beyond the epidemic threshold, favoring effective oncolytic viral therapy and immune-mediated tumor clearance.

7. Impact of different parameters on the reproduction number

The previous section showed that the parameters b and ξ influence the basic reproduction number $\mathcal{R}_0$, with b exhibiting a strong effect and ξ showing a moderate but still significant impact. Importantly, both parameters are directly related to the therapeutic components of the treatment: b captures the viral replication potential (burst size), while ξ represents the efficiency of MEK inhibitors. Given their clinical relevance, we further explore how simultaneous variations in b and ξ, while keeping the remaining parameter values fixed as listed in Table 1, affect the behavior of $\mathcal{R}_0$.

Since $\frac{\partial \mathcal{R}_0}{\partial b} = \frac{\beta K C_0}{2\mathcal{R}_0(\beta K C_0 + d_3)}$ and $\frac{\partial \mathcal{R}_0}{\partial \xi} = \frac{b\beta K \eta m d_3 d_4}{2\mathcal{R}_0(\eta\xi + d_4)^2(\beta K C_0 + d_3)^2}$ are always positive, then the burst size and the efficiency of MEK inhibitors have positive impacts on cancer control by increasing the reproduction number $\mathcal{R}_0$.

Figure 1 demonstrates that, in relation to reduced MEK inhibitors efficacy, a higher value of viral bursting size is required to increase $\mathcal{R}_0$ over 1. Figures $1-(b)$ and $1-(c)$ show that, regardless of the efficiency of MEK inhibitors, if the burst size is below a particular value, $\mathcal{R}_0$ will never be brought above 1, and hence, cancer cannot be controlled.

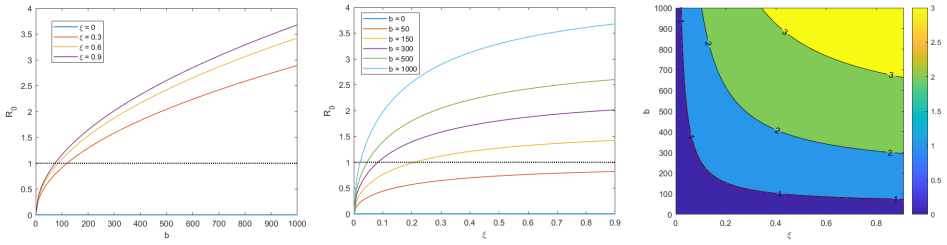

(a) $\mathcal{R}_0$ versus b with different values of ξ

(b) $\mathcal{R}_0$ versus ξ with different values of b

(c) Contour plot of $\mathcal{R}_0$ against b and ξ

Figure 1. Effect of burst size and the efficiency of MEK inhibitors on the basic reproduction number $\mathcal{R}_0$

Since m and d_3 are also important parameters that characterize the treatment's therapeutic effect, it is worthwhile to examine how their interaction with the burst size b influences the basic reproduction number $\mathcal{R}_0$.

The maximum number of CAR has a positive effect on cancer control by increasing the reproduction number $\mathcal{R}_0$ while the viral clearance rate always has a negative effect on cancer control, according to the expressions $\frac{\partial \mathcal{R}_0}{\partial m} = \frac{b\beta K \eta d_3}{2\mathcal{R}_0(\eta\xi + d_4)(\beta K C_0 + d_3)^2}$ and $\frac{\partial \mathcal{R}_0}{\partial d_3} = \frac{-b\beta K C_0}{2\mathcal{R}_0(\beta K C_0 + d_3)^2}$. According to Figure 2, the burst size must be larger to raise the mathematical $\mathcal{R}_0$ over 1 when the viral clearance rate (the maximum number of CAR) increases (decreases). Furthermore, regardless of the values of d_3

and m, the basic reproduction number $\mathcal{R}_0$ is greater than 1 if the value of b is bigger than $b^* = \frac{\beta K C_0 + d_3}{\beta K C_0}$.

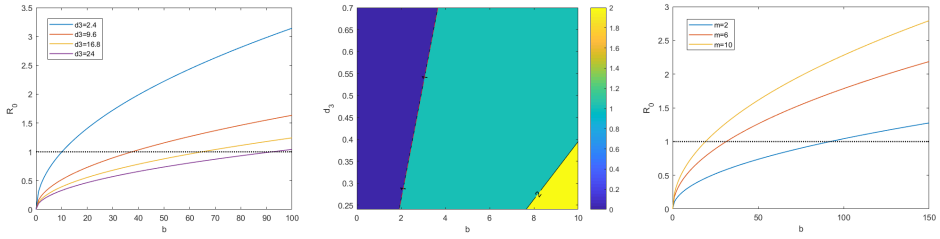

(a) $\mathcal{R}_0$ versus b with different values of d_3

(b) Contour plot of $\mathcal{R}_0$ against b and d_3

(c) $\mathcal{R}_0$ versus b with different values of m

Figure 2. Effect of burst size, maximum number of CAR, and viral clearance rate on the basic reproduction number $\mathcal{R}_0$

8. Stability region of equilibrium points with respect to the burst size b and the activation rate of NK cells α

In this section, we looked into the stability of equilibrium points under conditions when both the burst size b and the NK cell activation rate α are simultaneously varying. While the other parameters' values are as shown in Table 1, we varied b and α in the simulations to determine the stability of equilibrium points. The stability regions of equilibrium points were then shown in two-dimensional parameter space (α, b), as shown in Figure 3. For this purpose, we evaluated the eigenvalues of the Jacobian matrix at each equilibrium point by varying b from 0 to 1000 at a step size of 1, and varying α from 0 to 1.5×10^{-7} with a step size of 10^{-9}. Figure 3$-(a)$ shows that there are threshold values of b and α that are sufficient for a transition from the existence of one endemic equilibrium (NK cell-free equilibrium E_2) to the coexistence of two endemic equilibria (NK cell-free equilibrium E_2 and the presence of NK cells equilibrium E_3). The colored regions in Figure 3$-(b)$ stand for the following:

- The blue region is the set of (α, b) at which the Virus infection-free equilibrium E_1 is asymptotically stable.
- The red and green regions are the sets of (α, b) at which the Endemic equilibrium E_2 is asymptotically stable.
- The green region is the set of (α, b) at which the Endemic equilibrium E_3 is asymptotically stable (bistability).

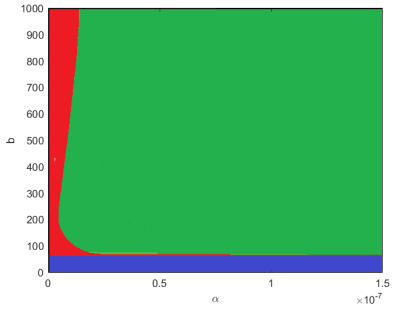

(a) E_1 exists at all regions; E_2 exists at the red and green regions, and E_3 exists at the green region.

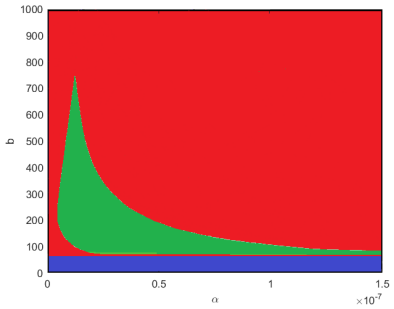

(b) E_1 is asymptotically stable at the blue region; E_2 is asymptotically stable at the red and green regions, and E_3 is asymptotically stable at the green region.

Figure 3. Existence and stability regions of equilibrium points E_1 , E_2 , and E_3 with respect to b and α.

9. Effect of activated NK cells on oncolytic virotherapy

We investigated how the parameters b and α have an impact on the equilibrium population of cancer cells. For experiment simulations, we measured the equilibrium populations of uninfected cancer cells and NK cells over b from 0 to 1000 with a step size of 1 with various values of α ($\alpha = 0.4 \times 10^{-7}$, $\alpha = 0.8 \times 10^{-7}$, $\alpha = 1.2 \times 10^{-7}$ and $\alpha = 1.6 \times 10^{-7}$) while the other parameters' values are indicated in Table 1. The equilibrium populations of uninfected cancer cells and NK cells were calculated as functions of b and then presented in Figure 4 as curves. From Figure 4$-(a)$, we see that the activation of NK cells starts at $b = b^*$ and the higher the value of α, the more significant this activation is.

Figure 4-(b) shows that, regardless of the value of α, for $b > b^*$, the population of uninfected cancer cells oscillates between two decreasing curves. The lower curve is the same for every value of α due to the fact that the endemic equilibrium E_2 is independent of α, whereas the four upper curves show that, the lower the value of α, the more successful the therapy is. We note that, the therapy always fails if b is lower than b^*. In conclusion, our numerical results show that larger values of α recruit more NK cells, resulting in the destruction of the infected cancer cell prior to oncolysis, which causes a reduction in the free virus particles and lowers the efficacy of oncolytic virotherapy.

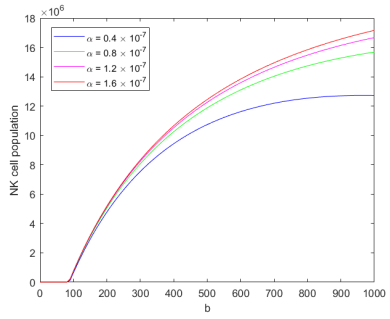

(a) The equilibrium population of NK cells over b

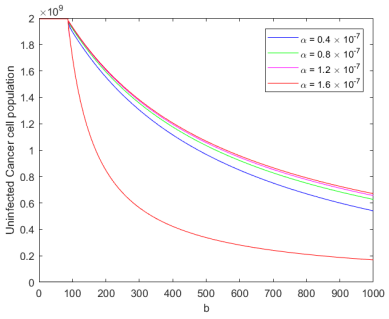

(b) The equilibrium population of uninfected cancer cells over b

Figure 4. The equilibrium populations of uninfected cancer cells and NK cells over the burst size b with different values of the activation rate of NK cells α.

10. Effect of the MEK inhibitors

We calculated the equilibrium populations of uninfected cancer cells and NK cells as functions of b (from 0 to 1000) with different values of ξ ($\xi = 0.1$, $\xi = 0.3$, $\xi = 0.5$, $\xi = 0.7$, and $\xi = 0.9$) to examine how the MEK inhibitors affect the equilibrium population of cancer cells. In two-dimensional parameter space (ξ, b), we plotted the existence regions of the equilibrium points. According to Figure 5, the existence of endemic equilibrium E_2 and E_3 requires a greater value of the virus's bursting size for lesser MEK inhibitor efficacy. Additionally, regardless of the effectiveness of MEK inhibitors, these endemic equilibriums will never be created if the burst size is below a particular value. Moreover, the values of ξ determine the number of equilibrium points by creating or destroying the presence of NK cells equilibrium E_3.

Figures 6 and 7 show that by improving the effectiveness of MEK inhibitors, we may increase the effectiveness of oncolytic virotherapy because, as the number of CAR molecules rises, the population of uninfected cancer cells becomes less important. Furthermore, for specific values of ξ (e.g., $\xi = 0.1$ and $\xi = 0.5$), MEK inhibitors prevent NK cell recruitment. By inhibiting MEK, these inhibitors can suppress the production of key chemoattractant cytokines and chemokines, such as CXCL10, CCL5, and IL-8, which are secreted by tumor cells and stromal cells in response to MAPK pathway activation [33, 34]. These signaling molecules play a crucial role in recruiting immune cells, including natural killer (NK) cells, to the tumor microenvironment. The MAPK/ERK signaling cascade, where MEK is a central kinase, is often hyperactivated in cancer and drives inflammation-associated gene expression. When MEK is inhibited, the downstream transcriptional activation of genes encoding chemoattractants is reduced. This leads to diminished chemotactic gradients in the tumor, thereby impairing NK cell migration and infiltration [33].

Biologically, this means that even if NK cells are activated systemically (e.g., via cytokines like IL-2 or IL-15), they may not be effectively recruited into the tumor if MEK signaling is suppressed. This has the consequence of reducing early clearance of virus-infected cancer cells, allowing oncolytic viruses more time to repli-

cate and induce tumor lysis. Thus, MEK inhibitors alter not just the cancer cell's intrinsic behavior, but also the composition and dynamics of the tumor immune microenvironment, leading to fewer signals for NK cells to migrate towards the tumor. This suppression enhances the effectiveness of the OV. In conclusion, MEK inhibitors neutralize the detrimental effects of NK cell hyperactivation by suppressing chemoattractant-mediated recruitment and reshaping the tumor microenvironment in a manner that supports OV efficacy. This dual role - limiting harmful NK cell infiltration while preserving essential antitumor activity - underscores the therapeutic value of MEK inhibitors in combination strategies.

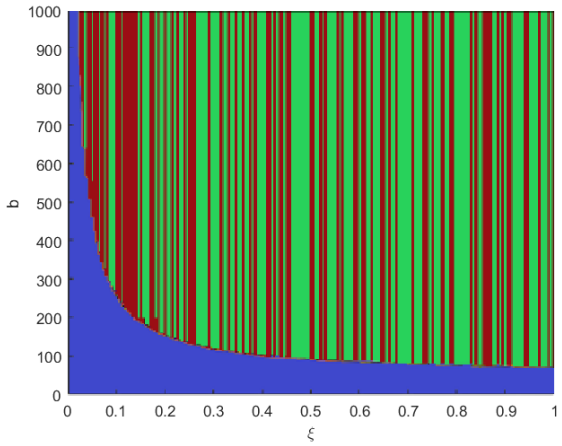

Figure 5. Existence regions of equilibrium points E_1, E_2, and E_3 with respect to b and ξ. E_1 exists at all regions, E_2 exists at the red and green regions, and E_3 exists at the green region.

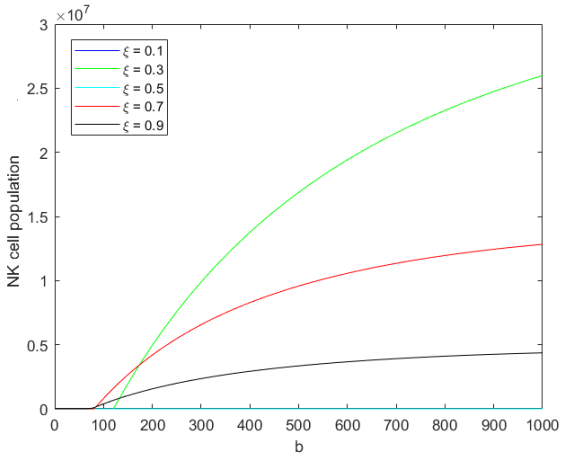

Figure 6. The equilibrium population of the NK cells with different values of ξ

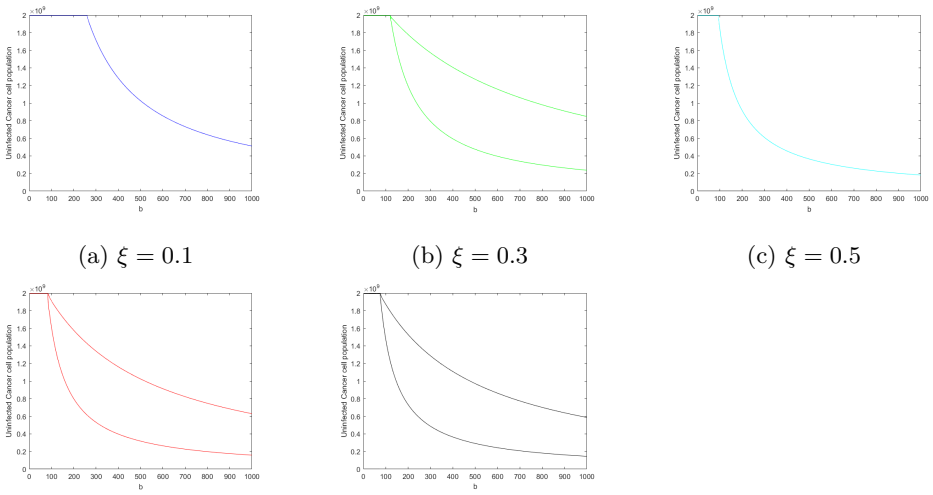

(a) $\xi = 0.1$ (b) $\xi = 0.3$ (c) $\xi = 0.5$

(d) $\xi = 0.7$ (e) $\xi = 0.9$

Figure 7. The equilibrium population of the uninfected cancer cells with different values of ξ

11. Conclusion

In order to simulate the combination of oncolytic viral therapy and MEK inhibition for the treatment of glioma, a nonlinear mathematical model was provided in this article. First, we checked the well-posedness of our model. Then, we established the existence and boundedness of solutions. The dynamics of the population among NK cells, uninfected cancer cells, infected cancer cells, oncolytic viruses, and the CAR molecules on the surface of the cancer cells were then analyzed. To do this, we searched for equilibrium points and examined their local stability. Thus, the existence and stability of the equilibria depend on b,α, and ξ, and our two-dimensional diagrams offer an encouraging result in identifying the ideal parameters for effective therapy. The simulations show that there are threshold values for the burst size (b), NK cell activation rate (α), and MEK inhibitor efficacy (ξ) at which there is a change from the existence of one endemic equilibrium (NK cell-free equilibrium E_2) to the coexistence of two endemic equilibria (NK cell-free equilibrium E_2 and the presence of NK cells equilibrium E_3). Additionally, as the rate of NK cell activation increases, oncolytic virotherapy loses its effectiveness because the infected cancer cells are eliminated before oncolysis. Therefore, when NK cell activation increases, higher virus bursting rates are needed to achieve the same level of uninfected cancer cells, whereas low viral bursting rates, regardless of α values, result in therapy failure. Afterwards, we looked into how oncolytic virotherapy was affected by MEK inhibition. As a result, the value of the virus bursting size needed for the existence of endemic equilibrium E_2 and E_3 increases as MEK inhibitor efficacy decreases. Additionally, there is a threshold value of the burst size (b) for which certain endemic equilibria can never exist, regardless of how effective MEK inhibitors are. It implies that we will not be able to control cancer. Furthermore, the values of ξ determine the number of equilibrium points by creating or destroying the presence of NK cells equilibrium E_3. The simulations demonstrate that by making MEK inhibitors more effective, we can reduce the level of uninfected cancer cells,

and consequently increase the effectiveness of oncolytic virotherapy and neutralize the negative effect of NK cell activation. In addition, for some values of ξ, these inhibitors may even prevent the recruitment of NK cells, making OV more effective.

Declarations

Conflict of interest The authors declare no conflict of interest.

References

[1] J.-W. Choi, Y. S. Lee, C.-O. Yun, S. W. Kim. *Polymeric oncolytic adenovirus for cancer gene therapy*, J Control Release, 2015, 219: 181–191.

[2] K. J. Mahasa, L. De Pillis, R. Ouifki, A. Eladdadi, P. Maini, A.-R. Yoon, C.-O. Yun. *Mesenchymal stem cells used as carrier cells of oncolytic adenovirus results in enhanced oncolytic virotherapy*, Sci Rep, 2020, 10(1): 425.

[3] A. C. Filley, M. Dey. *Immune system, friend or foe of oncolytic virotherapy?*, Front Oncol, 2017, 7: 106.

[4] T. Shi, X. Song, Y. Wang, F. Liu, J. Wei. *Combining oncolytic viruses with cancer immunotherapy: establishing a new generation of cancer treatment*, Front Immunol, 2020, 11: 683.

[5] A. Marchini, E. M. Scott, J. Rommelaere. *Overcoming barriers in oncolytic virotherapy with HDAC inhibitors and immune checkpoint blockade*, Viruses, 2016, 8(1): 9.

[6] A.-R. Yoon, J. Hong, Y. Li, H. C. Shin, H. Lee, H. S. Kim, C.-O. Yun. *Mesenchymal stem cell–mediated delivery of an oncolytic adenovirus enhances antitumor efficacy in hepatocellular carcinoma*, Cancer Res, 2019, 79(17): 4503–4514.

[7] R. Bhat, J. Rommelaere. *Emerging role of natural killer cells in oncolytic virotherapy*, ImmunoTargets Ther, 2015, : 65–77.

[8] E. Y. L. Leung, D. P. Ennis, P. R. Kennedy, C. Hansell, S. Dowson, M. Farquharson, P. Spiliopoulou, J. Nautiyal, S. McNamara, L. M. Carlin, et al. *NK cells augment oncolytic adenovirus cytotoxicity in ovarian cancer*, Mol Ther Oncolytics, 2020, 16: 289–301.

[9] D. Wodarz, S. Sierro, P. Klenerman. *Dynamics of killer T cell inflation in viral infections*, J R Soc Interface, 2007, 4(14): 533–543.

[10] N. S. Senekal, K. J. Mahasa, A. Eladdadi, L. de Pillis, R. Ouifki. *Natural killer cells recruitment in oncolytic virotherapy: a mathematical model*, Bull Math Biol, 2021, 83(7): 75.

[11] A. L. De Matos, L. S. Franco, G. McFadden. *Oncolytic viruses and the immune system: the dynamic duo*, Mol Ther Methods Clin Dev, 2020, 17: 349–358.

[12] E. Y. L. Leung, I. A. McNeish. *Strategies to optimise oncolytic viral therapies: the role of natural killer cells*, Viruses, 2021, 13(8): 1450.

[13] D. Kim, D.-H. Shin, C. K. Sung. *The optimal balance between oncolytic viruses and natural killer cells: a mathematical approach*, Mathematics, 2022, 10(18): 3370.

[14] S. M. Chang, I. F. Parney, W. Huang, F. A. Anderson, A. L. Asher, M. Bernstein, K. O. Lillehei, H. Brem, M. S. Berger, E. R. Laws, et al. *Patterns of care for adults with newly diagnosed malignant glioma*, JAMA, 2005, 293(5): 557–564.

[15] G. Wollmann, K. Ozduman, A. N. Van Den Pol. *Oncolytic virus therapy of glioblastoma multiforme–concepts and candidates*, Cancer J (Sudbury, Mass.), 2012, 18(1): 69.

[16] S. Nandi, M. S. Lesniak. *Adenoviral virotherapy for malignant brain tumors*, Expert Opin Biol Ther, 2009, 9(6): 737–747.

[17] I. V. Ulasov, A. V. Borovjagin, B. A. Schroeder, A. Y. Baryshnikov. *Oncolytic adenoviruses: a thorny path to glioma cure*, Genes Dis, 2014, 1(2): 214–226.

[18] M. Kim, L. A. Sumerel, N. Belousova, G. R. Lyons, D. E. Carey, V. Krasnykh, J. T. Douglas. *The coxsackievirus and adenovirus receptor acts as a tumour suppressor in malignant glioma cells*, Br J Cancer, 2003, 88(9): 1411–1416.

[19] R. Zurakowski, D. Wodarz. *Model-driven approaches for in vitro combination therapy using ONYX-015 replicating oncolytic adenovirus*, J Theor Biol, 2007, 245(1): 1–8.

[20] B. I. Camara, H. Mokrani, E. K. Afenya. *Mathematical modeling of glioma therapy using oncolytic viruses*, Math Biosci Eng, 2013, 10(3): 565–578.

[21] M. K. Nono, E. B. M. Ngouonkadi, S. Bowong, H. B. Fotsin. *Synergistic effects of oncolytic adenovirus and MEK inhibitors on glioma treatment dynamics: Analysis and optimal control*, Appl Math Sci, 2020, 14(16): 781–800.

[22] A. Friedman, J. P. Tian, G. Fulci, E. A. Chiocca, J. Wang. *Glioma virotherapy: effects of innate immune suppression and increased viral replication capacity*, Cancer Res, 2006, 66(4): 2314–2319.

[23] T. Linsenmann, A. Jawork, T. Westermaier, G. Homola, C. M. Monoranu, G. H. Vince, A. F. Kessler, R.-I. Ernestus, M. Lohr. *Tumor growth under rhGM-CSF application in an orthotopic rodent glioma model*, Oncol Lett, 2019, 17(6): 4843–4850.

[24] K. W. Okamoto, P. Amarasekare, I. T. D. Petty. *Modeling oncolytic virotherapy: Is complete tumor-tropism too much of a good thing?*, J Theor Biol, 2014, 358: 166–178.

[25] Y. Kim, J. Y. Yoo, T. J. Lee, J. Liu, J. Yu, M. A. Caligiuri, B. Kaur, A. Friedman. *Complex role of NK cells in regulation of oncolytic virus–bortezomib therapy*, Proc Natl Acad Sci USA, 2018, 115(19): 4927–4932.

[26] K. Jacobsen, L. Russell, B. Kaur, A. Friedman. *Effects of CCN1 and macrophage content on glioma virotherapy: A mathematical model*, Bull Math Biol, 2015, 77: 984–1012.

[27] R. Mandale, A. Kumar, D. K. K. Vamsi, P. K. Srivastava. *Dynamics of an infectious disease in the presence of saturated medical treatment of Holling type III and self-protection*, Journal of Biological Systems, 2021, 29(2): 245–289.

[28] S. H. Strogatz. *Nonlinear Dynamics and Chaos: With Applications to Physics, Biology, Chemistry, and Engineering*, Chapman and Hall/CRC, 2024.

[29] V. V. Filippov. *Basic Topological Structures of Ordinary Differential Equations*, Mathematics and Its Applications, vol.432, Springer, 2013.

[30] S. Sastry. *Introduction to control theory and applications*, Appl Math Sci, 2018, 12(2): 303–328.

[31] C. Castillo-Chavez, B. Song. *Dynamical models of tuberculosis and their applications*, Math Biosci Eng, 2004, 1(2): 361–404.

[32] N. Chitnis, J. M. Hyman, J. M. Cushing. *Determining important parameters in the spread of malaria through the sensitivity analysis of a mathematical model*, Bull Math Biol, 2008, 70: 1272–1296.

[33] J. S. C. Arthur, S. C. Ley. *Mitogen-activated protein kinases in innate immunity*, Nat Rev Immunol, 2013, 13(9): 679–692.

[34] S. Gentile, N. Eskandari, M. A. Rieger, B. D. Cuevas. *MEKK1 regulates chemokine expression in mammary fibroblasts: implications for the breast tumor microenvironment*, Front Oncol, 2021, 11: 609918.